Improved Quasi-Chemical Equation of State Based on Energy and Density Fluctuations in the Small System Grand Canonical Ensemble†

Christopher J. Roberts*

Department of Chemical Engineering, Colburn Laboratory, University of Delaware, Newark, Delaware 19716

Received: June 30, 2004; In Final Form: August 19, 2004

A quasi-chemical (QC) model of one-component fluids is considered that circumvents limitations of traditional QC treatments by incorporating "boundary" interactions—those interactions that involve molecules both external and internal to the fundamental cells or subvolumes inherent in QC fluid theories. This is achieved by including correlations between the energy and density of the subcells and the surrounding fluid, based on a representation of configurational probabilities within the small system grand canonical ensemble, and motivated in part by the behavior of such correlations observed in molecular simulations of a simple body-centered cubic lattice gas with nearest-neighbor attractions (bcc-LG). Energy and density correlations are included at an athermal level in the present work. The resulting model is found to give significantly improved predictions of the effects of temperature on local density fluctuations compared to the case in which such correlations are neglected, with results in semiquantitative agreement with those from molecular simulations. Despite only semi-quantitative agreement at the level of subvolume density fluctuations versus temperature, the resulting equation of state (EoS) is dramatically improved over traditional treatments in which boundary interactions are neglected. The QC EoS with boundary interactions gives predictions in excellent agreement with simulated bcc-LG vapor−liquid phase boundaries at $T/T_c < 0.82$. As expected due to the limited subcell dimensions, predictions are in poorer agreement as T_c is approached. In contrast, the QC model without boundary interactions predicts no phase separation at positive temperatures.

1. Introduction

The development and refinement of accurate, yet computationally tractable, liquid state theories has been a long-standing objective in statistical thermodynamics of condensed matter, as well as in applied physical chemistry and molecular thermodynamics. The motivation for this is highlighted by the increasing impetus to gain improved descriptions of complex liquids of biological interest, in which explicit incorporation of molecular solvents will likely remain a significant challenge for direct simulation of large-scale and long-time-scale macromolecular processes.[1,2] For any theory or model, it is hoped that a balance may be struck between a simple and insightful framework based on qualitative and physically meaningful molecular insights and an ability to quantitatively reproduce, and even predict, physical properties over a range of temperatures, pressures, and compositions. Approximate theories and models are sought to achieve these goals at low computational cost and ease of practical application to complex systems, but often require sacrifices in quantitative predictability. Explicit molecular simulation techniques and formal, exact theories provide useful testing grounds for approximate theories but are currently limited in their direct applicability to more complex systems due to prohibitive computational costs.[3−29] These limitations are exacerbated when global thermodynamic behavior is sought, for example, if such calculations must be repeated for each different state point of interest. The work reported here is first stage in the development of a relatively simple, general approach for obtaining analytical, semiquantitative, and quantitative predictions of the global thermodynamics and phase behavior of complex single- and multicomponent fluids.

Key underpinnings to a number of successful theories for liquids, and the models that result, include the roles of local density fluctuations and the work of cavity formation. Both of these contributions are intimately tied to the fluid's free energy, or, equivalently, its equation of state (EoS), and to its solvent properties.[3,4,30,31] These effects can often be treated analytically or semi-analytically; exactly in some idealized cases, but most often at a variety of levels of approximation.[3−7,13−19,22,26] For complex fluids and their mixtures, highly orientation-dependent interactions and nontrivial correlations in local density, composition, and energy are anticipated to play strong roles. These contributions are incorporated either explicitly at the model formulation stage[9−11,14,21−23] or implicitly, e.g., through correlation functions or other system-specific a priori (molecular) information obtained from experiment or molecular simulations of the liquid of interest.[5,6,8,12,13,20] Of course, increasing computational power and ongoing efforts toward the development of more sophisticated and efficient simulation methods[32−35] to estimate free energies directly from molecular simulations offer a complement to more analytical approaches.

The work reported here builds from a number of key advances alluded to above. This includes recent work on quasi-chemical (QC) theories of liquids and their mixtures[7,9−11,19,21] combined with treatments of "boundary" effects on local cell density and energy distribution functions in the small system grand canonical ensemble (SSGCE).[15−17,30] A hybrid approach is adopted here, based formally on an analytical approximation for the partition

† Part of the special issue "Frank H. Stillinger Festschrift".

* E-mail: roberts@che.udel.edu.

10.1021/jp047123g CCC: $27.50 © 2004 American Chemical Society
Published on Web 10/05/2004

function, but utilizing explicit molecular simulations to provide certain inputs to the analytical model. Specifically, a traditional QC fluid model[7,11] is revisited from the perspective of the SSGCE in order to include interactions between subcells comprising the fluid. This is done by including correlations between energy and density of the subcells and of the surrounding fluid. Some aspects of this treatment are similar in spirit to recent work on quasi-Gaussian entropy theory approaches,[24,25] in that knowledge of the distribution of energy states at a set of reference conditions is used to extrapolate EoS predictions to lower temperatures for simple liquids. Recent applications of QC treatments to calculate density fluctuations[19] and solute excess chemical potentials[26] in simple (hard-sphere) liquids, including the introduction of an empirical self-consistent field to account for density correlations at the subvolume boundary,[26] are also notable. Although presented in a somewhat different mathematical framework, the latter treatments are consistent with earlier presentations of the extended QC theory without boundary interactions,[7,11] and with its adaptation here in which density and energy correlations at the boundary are included.

The approach presented here is intended to provide the first stages of a general framework in which knowledge of the density and energy fluctuations at one or a small number of state points can be used to infer the equation of state for pure fluids as well as arbitrarily complex mixtures across broad ranges of temperature, density, and composition. The present report focuses solely on the theory and model approximations for a simple, single-component fluid represented by a body-centered cubic lattice gas with nearest-neighbor attractions (bcc-LG). The bcc-LG provides a convenient and sufficiently rich system for initial tests and illustrations of the QC theory including cell boundary energy−density correlations. It is also commensurate with coarse-grained lattice fluid descriptions of water[11,37] and aqueous solutions of sp^3 hybridized solutes and cosolvents currently being pursued in parallel with the work reported here.

Energy−density correlations are included at this stage in an athermal manner. They are found to provide significant improvements to the predictions of the effects of temperature on local density fluctuations and dramatic improvements to the QC equation of state, characterized in terms of predictions of vapor−liquid equilibrium (VLE) as a function of temperature. In the present work, it is found that the neglect of such boundary interactions prevents the traditional QC model from predicting VLE at positive temperatures, while the inclusion of those interactions provides quantitative agreement with direct molecular simulation.

2. Monte Carlo Simulations and Subvolume Statistics in the bcc-LG Model

A one-component body-centered cubic lattice gas with nearest-neighbor attractions (bcc-LG) was simulated using conventional Monte Carlo methods.[38] As is common in lattice fluid models, each site was either vacant or occupied by a single particle, to emulate the analogous hard-sphere or repulsive cores in nonlattice models. Nearest-neighbor (*nn*) pairs contribute an additive, attractive contribution, $-\epsilon$, to the potential energy of the fluid. The Hamiltonian of this system is

$$H = -\epsilon \sum_{\langle ij\rangle=nn} s_i s_j \qquad (1)$$

with s_i denoting the occupation variable of the ith site. $s_i = 0$ for a vacant site and 1 for an occupied site. The symbol $\langle ij\rangle$ in eq 1 denotes the sum is over only distinguishable *nn* pairs. For use below and in later sections, the following dimensionless variables are introduced. $T^* \equiv kT/\epsilon$ is the dimensionless temperature, with T being the absolute temperature and k denoting Boltzmann's constant. υ_0 is the volume per site, N is the number of filled sites or the number of particles, $B \equiv V\upsilon_0^{-1}$ is the dimensionless volume or, equivalently, the total number of sites, and $\rho \equiv N\upsilon_0/V = N/B$ is the dimensionless density or fractional occupancy on the lattice.

Canonical ensemble (*NVT*) simulations were performed using a Metropolis Monte Carlo (MC) algorithm utilizing single particle translational moves on a 2000-site ($10 \times 10 \times 20$) lattice[39] with a standard minimum image convention.[38] Typical equilibration stages were from 5×10^4 to 10×10^4 MC trials per particle. Ensemble averaging was performed over a range of durations, with a minimum of 2.5×10^5 MC trials per particle. For purposes of generating histograms of subvolume density and energy fluctuations (see below and section 4), significantly longer ensemble averaging runs were used, with typical durations ranging from 10^6 to 10^7 MC trials per particle. These may have been unnecessarily long, as a systematic evaluation of the minimum duration needed to provide converged probability distributions was beyond the scope of this study.

Fluctuations in number density and energy within subvolumes or subcells of the 2000-site canonical system were measured by collecting histograms of the number of occupied sites, the number of *nn* contacts between particles within the subcell, and the number of *nn* contacts involving one particle within and one particle external to the subcell. These quantities are all that are needed to calculate, respectively, the subcell density, energy "internal" to the cell (E_n in section 3), and boundary or surface energy (E_σ in section 3). The histograms were collected for 16-site cubic subcells stenciled randomly throughout the system during ensemble averaging, with a frequency ranging from one stencil per MC trial to one stencil per ten MC trials. Thus, upward of 10^{10} subcell placements were made in the longest simulations. A 16-site cubic subcell can be represented as two diagonally interpenetrating bcc unit cells. For this geometry, it can be shown that the maximum numbers of internal and boundary *nn* contacts are 27 and 74, respectively.

The $T^*-\rho$ vapor−liquid phase boundaries for the bcc-LG model were determined via a transition matrix Monte Carlo (TMMC) approach in the grand canonical (GC) ensemble, according to the protocol described in recent reports,[32,33] along with standard isothermal histogram reweighting techniques.[32,40] In brief, the bcc-LG was simulated in the GC ensemble, using a 128-site periodic box and purely insertion and deletion steps. The smaller box size was chosen for two reasons. The first was to make large density fluctuations facile in the vicinity of vapor−liquid equilibrium (VLE), and thereby improve the computational efficiency with which densities spanning VLE were sampled.[32,33] The second was to ensure that the simulation sampled from only states representative of homogeneous fluids; that is, the 2000-site box was empirically found to be sufficiently large to permit (frustrated) phase separation to occur within its boundaries. This was evidenced by the observation that, at temperatures below approximately the critical temperature, the subvolume density profile became bimodal, with the modes splitting to higher and lower densities as temperature was lowered further. Although such bimodal subcell distributions have been used previously to estimate the location of phase boundaries,[37,41−43] they are not reliable for highly quantitative determination of the equilibrium values.[41,42]

The TMMC procedure consists of sampling within a conventional GCMC simulation, except that a histogram is kept of trial insertion and deletion moves and their associated acceptance probabilities rather than the resulting visited states. This histogram is periodically used to generate an estimate of the (macrostate) probability of observing a given (bulk) density, ρ, or occupancy, N, denoted $\Pi(N)_{\text{est}}$. The estimated $\Pi(N)$ values are then utilized to impose a non-Boltzmann weighting to bias the simulation[32] to sample from lower-probability N values, thereby efficiently and continually improving the estimate of $\Pi(N)$ throughout the simulation. The simulations were run at a selected T^* value and a reduced chemical potential ($\mu^* = \mu/\epsilon$) until a sufficiently accurate estimate of $\Pi(N; T^*, \mu^*)$ was achieved to ensure uniform sampling in N. Histogram reweighting techniques[32,40] were employed to identify the value of μ^* at coexistence, as determined by an equal-area construction for the liquid and vapor modes of $\Pi(N; T^*, \mu^* = \mu^*_{\text{coex}})$. The average values of ρ for the vapor and liquid modes are taken as the bulk densities at coexistence.[32]

3. Small System Grand Canonical Ensemble and Quasi-Chemical Model Including Boundary Interactions

Subvolume or Cell Probabilities in the SSGCE. We begin with an expression for the canonical partition function of a single component in three dimensions, in which a subvolume, v, within V is treated explicitly. The nomenclature is adapted somewhat from the original references[15,30] for reasons of consistency with results anticipated from later in this section.

$$Q(N, V, T) = \frac{1}{N!}\sum_{n=0}^{N}\frac{N!}{(N-n)!n!\Lambda^{3N}}\int_{V-v}(\mathrm{d}\tau)^{N-n}e^{-\beta E_{N-n}}\int_{v}(\mathrm{d}\tau)^{n}e^{-\beta(E_n+E_\sigma)} \quad (2)$$

In eq 2, Λ is the de Broglie wavelength, $\beta = 1/kT$, n denotes the number of particle centers within v, $N-n$ those in $V-v$, $(\mathrm{d}\tau)^n$ denotes the volume elements of integration of the n particles within the confines of v, and $(\mathrm{d}\tau)^{N-n}$ is defined analogously for the $N-n$ particles confined to $V-v$. E_n is the contribution to the total potential energy due to interactions between only those particles residing within v, E_{N-n} is the contribution due to interactions between those particles residing within $V-v$, and E_σ is the "boundary energy", or surface energy, due to interactions that involve both molecules in v and $V-v$. This last point should be highlighted. E_σ is by definition a function simultaneously of the positions of particles within v and those within $V-v$.

The probability of observing a subvolume configuration consisting of n_j particles with a specific value of E_n, denoted $E_{n,j}$, within an interval $\mathrm{d}E$ is given formally by

$$p(n_j, E_{n,j})\,\mathrm{d}E = N!^{-1}Q^{-1}\frac{N!}{(N-n_j)!n_j!\Lambda^{3N}}\int_{V-v}(\mathrm{d}\tau)^{N-n_j}e^{-\beta E_{N-nj}} \times \int_{v}(\mathrm{d}\tau)^{n_j}e^{-\beta E_\sigma}e^{-\beta E_n(\tau^{nj})}\int_{E_{n,j}-\mathrm{d}E/2}^{E_{n,j}+\mathrm{d}E/2}\mathrm{d}E'\,\delta(E'-E_n(\tau^{n_j})) \quad (3)$$

In eq 3, δ denotes the Dirac delta function and the last integral selects only those configurations in which E_n lies within $E_{n,j} \pm \mathrm{d}E/2$. It follows that the probability of observing exactly n particles in v, irrespective of the energy of the subvolume configuration, is given by

$$\begin{aligned} p(n_j = n) &= \int_{-\infty}^{\infty}\mathrm{d}E_{n,j}\,p(n_j = n, E_{n,j}) \\ &= Q^{-1}\frac{1}{(N-n)!n!\Lambda^{3N}}\int_{V-v}(\mathrm{d}\tau)^{N-n}e^{-\beta E_{N-n}}\int_{v}(\mathrm{d}\tau)^{n}e^{-\beta E_\sigma}e^{-\beta E_n(\tau^n)} \end{aligned} \quad (4)$$

For the purposes of the EoS calculations described in the next subsection, we require $p(n_j, E_{n,j})\mathrm{d}E$, rather than $p(n)$. In what follows, we use $E_{n,j}$ to denote the jth subvolume configuration's E_n value, with the surrounding interval $\mathrm{d}E$ about $E_{n,j}$ being understood. With this convention, the subvolume degeneracy associated with $(n_j, E_{n,j})$ is given formally by

$$\omega_v(n_j, E_{n,j}) = \frac{1}{n!}\int_{v}(\mathrm{d}\tau)^{n_j}\int_{E_{n,j}-\mathrm{d}E/2}^{E_{n,j}+\mathrm{d}E/2}\mathrm{d}E'\,\delta(E'-E_n(\tau^{n_j})) \quad (5)$$

Multiplying and dividing the numerator in eq 4 by ω_v gives

$$p(n_j, E_{n,j}) = Q^{-1}\frac{1}{(N-n_j)!\Lambda^{3N}}\omega_v(n_j, E_{n,j})e^{-\beta E_{n_j}} \times \int_{V-v}(\mathrm{d}\tau)^{N-n_j}e^{-\beta E_{N-n_j}}\langle e^{-\beta E_\sigma}\rangle^{(v)}_{E_{n,j},\tau^{N-nj}} \quad (6)$$

with

$$\langle e^{-\beta E_\sigma}\rangle^{(v)}_{E_{n,j},\tau^{N-n_j}} = \omega_v{}^{-1}n!^{-1}\int_{v}(\mathrm{d}\tau)^{n_j}\int_{E_{n,j}-\mathrm{d}E/2}^{E_{n,j}+\mathrm{d}E/2}\mathrm{d}E'\,\delta(E'-E_n(\tau^{n_j}))e^{-\beta E_\sigma(\tau^{n_j},\tau^{N-n_j})} \quad (7)$$

denoting the average Boltzmann factor for the boundary energy associated with a subvolume configuration having n_j and $E_{n,j}$, and a specific arrangement of the $N-n_j$ particles external to v. The dependence of E_σ on the positions of the n_j and $N-n_j$ particles is indicated explicitly in eq 7.

To simplify the nomenclature, and to illustrate parity with conventional QC formalisms later in this section, we let j denote the set $[n_j, E_{n,j}]$ that defines the jth subvolume configuration, and $\omega_j = \omega_v(n_j, E_{n,j})$. Equation 6 can then be rewritten as

$$p_j = \frac{\frac{1}{(N-n_j)!}\omega_j e^{-\beta E_{nj}}\int_{V-v}(\mathrm{d}\tau)^{N-n_j}e^{-\beta E_{N-nj}}\langle e^{-\beta E_\sigma}\rangle^{(v)}_{E_{n,j},\tau^{N-n_j}}}{\sum_j\frac{1}{(N-n_j)!}\omega_j e^{-\beta E_{nj}}\int_{V-v}(\mathrm{d}\tau)^{N-n_j}e^{-\beta E_{N-nj}}\langle e^{-\beta E_\sigma}\rangle^{(v)}_{E_{n,j},\tau^{N-n_j}}} \quad (8)$$

or more simply

$$p_j = \frac{\omega_j e^{-\beta E_{nj}}Q'_j\langle\langle e^{-\beta E_\sigma}\rangle^{(v)}_{E_{n,j},\tau^{N-n_j}}\rangle^{(V-v)}}{\sum_j\omega_j e^{-\beta E_{nj}}Q'_j\langle\langle e^{-\beta E_\sigma}\rangle^{(v)}_{E_{n,j},\tau^{N-n_j}}\rangle^{(V-v)}} \quad (9)$$

with Q'_j defined as

$$Q'_j \equiv \frac{1}{(N-n_j)!}\int_{V-v}(\mathrm{d}\tau)^{N-n_j}e^{-\beta E_{N-n_j}} \quad (10)$$

Finally, defining the effective or average boundary energy of the jth configuration

$$E'_{\sigma,j} \equiv -kT \ln\langle\langle e^{-\beta E_\sigma}\rangle^{(v)}_{E_j,\tau^{N-n_j}}\rangle^{(V-v)} \tag{11}$$

and substituting in eq 9 gives

$$p_j = \frac{\omega_j e^{-\beta E_j} Q'_j}{\sum_j \omega_j e^{-\beta E_j} Q'_j} = \omega_j \psi_j \tag{12}$$

with

$$E_j \equiv E_{n,j} + E'_{\sigma,j} \tag{13}$$

The last equality in eq 12 effectively defines ψ_j for use in QC models[7,11] such as that described in the subsection below. The above relations are formally exact, but it should be noted that $E_{\sigma,j}$ is, in general, a function not only of j but also of temperature and density, as it results from an ensemble average over the degrees of freedom of the $N - n_j$ particles in $V - v$ for fixed n_j and $E_{n,j}$ values, at a given N, V, and T. $E_{n,j}$ can, in principle, be known or enumerated a priori as the set $\{n_j, E_{n,j}\}$ are independent of the state point at which the fluid EoS is evaluated. $E_{\sigma,j}$ requires approximation(s) or a means to evaluate it from simulation. One possible procedure to obtain $E_{\sigma,j}$ is explained below and utilized for the calculations presented in section 4. Note that ψ_j implicitly contains contributions from both $E_{n,j}$ and $E_{\sigma,j}$. The discussion and derivations below indicate how each ψ_j can be evaluated once the sets of ω_j and E_j (i.e., both $E_{n,j}$ and $E_{\sigma,j}$) are known.

Extended Quasi-Chemical Fluid Model. Some of the derivations below are formally similar to earlier presentations.[7,11] Only key steps will therefore be included for the sake of clarity with respect to determining two key quantities: the equation of state, particularly vapor−liquid phase equilibrium predictions, and $p(n, E)$ for a given v at a specified temperature and density.

In the QC formulation, the equilibrium configurations of the macroscopic fluid are assumed to be well described by partitioning the macroscopic volume, V, into N_c subcells. The ensemble of macroscopic system configurations is approximated as a randomly placed set of the N_c subcells, with $p_j N_c$ cells, on average, in configuration j. The resulting partition function can be written as

$$\begin{aligned} Q(N, V, T) &= C_0 \exp(-\beta N_c \sum_j \omega_j \psi_j [E_j + kT \ln \psi_j]) \\ &= C_0 \prod_j \exp(-\beta N_c \omega_j \psi_j \{E_j + kT \ln \psi_j\}) \end{aligned} \tag{14}$$

in which j represents the set $[n_j, E_j]$ (rather than n_j, $E_{n,j}$ as in the preceding section) and C_0 is a constant chosen to ensure Q is accurate in some limiting case, typically the infinite temperature or athermal limit.[7,11,30] It follows readily from eq 14 that the Helmholtz free energy density, $a \equiv A/V$, is given by

$$a = -v^{-1} \sum_j \omega_j \psi_j \left(E_j + kT \ln \psi_j - kT \frac{\psi_{j,\mathrm{ref}}}{\psi_j} \ln \psi_{j,\mathrm{ref}}/\psi_j \right) + a_{\mathrm{ref}} \tag{15}$$

with $v \equiv N_c/V$ defining the volume of a subcell. If the sets of ω_j and ψ_j are known, the free energy of the system is readily calculated as well as the resulting equation of state (EoS) via the appropriate derivatives. The set of p_j, or equivalently $p(n_j, E_j)$ and $p(n)$, can also then be calculated. Note that there are two additional constraints that are conventionally imposed on the basis of physical grounds. The first is normalization of $\{p_j\}$

$$\sum_j p_j = 1 \tag{16a}$$

The second is the requirement that the average cell density equals the bulk density

$$\sum_j p_j \rho_j = \rho \tag{16b}$$

with $\rho_j = n_j/v$. If m_c denotes the total number of distinguishable cell configurations, across all $\{n_j, E_j\}$, at this point one has $2m_c$-2 unknowns which are in principle arbitrary. There are a number of possible approaches to make a solution to this problem tractable.[44] In the one pursued here, we seek to enable the calculation of both $\{p_j\}$ and $\{\psi_j\}$, which are required for the EoS. With this in mind, it is convenient to apply the following equilibrium constraints.

$$\left(\frac{\partial a}{\partial \psi_j}\right)_{T,\rho,\psi_{k\neq j,0,1}} = 0, j \neq 0, 1 \tag{17}$$

The values of $j = 0$, 1 denote arbitrarily selected subcell configurations that are previously constrained due to a need to satisfy eq 16. The only limitations on their choice in the case of a single-component fluid is that they must have different subvolume densities.[11] Applying the chain rule to eq 17, subject to eq 16, the constraints implied by eq 17 can be re-expressed algebraically for a single-component fluid as[11]

$$\ln\frac{\psi_j}{\psi_0} = \left(\frac{\rho_j - \rho_0}{\rho_1 - \rho_0}\right) \ln r_1 - \beta\left[E_j - E_0\left(\frac{\rho_j - \rho_1}{\rho_0 - \rho_1}\right) - E_1\left(\frac{\rho_j - \rho_0}{\rho_1 - \rho_0}\right)\right], j \neq 0, 1 \tag{18}$$

with $r_1 \equiv \psi_1/\psi_0$. Thus, we are left with m_c unknowns at a given (T, ρ). If one knows $\{\omega_j\}$, the problem reduces to one of identifying the value of r_1 that provides the correct bulk density at a given temperature, that is, solving

$$\rho = \frac{\omega_0\rho_0 + \omega_1\rho_1 r_1 + \sum_{j>1} \omega_j \rho_j \frac{\psi_j}{\psi_0}(r_1, T)}{\omega_0 + \omega_1 r_1 + \sum_{j>1} \omega_j \frac{\psi_j}{\psi_0}(r_1, T)} \tag{19}$$

for r_1. Historically, the above approach was hampered due to the need to enumerate, typically "by hand", the m_c subcell degeneracies $\{\omega_j\}$ in order to make the QC approach tenable. This also limited its utility because such enumeration inevitably required both a discretized (e.g., lattice) description of the fluid and a rather small v value. For example, a v value ~10 or more times the characteristic volume of a molecule was considered all but prohibitive for enumeration unless significant simplifications could be made.[7,9−11,21] The approach described below seeks to circumvent such limitations.

Before doing so, it is worth noting that the set $\{\omega_j\}$ in eqs 14, 15, and 19 is independent of $E_{\sigma,j}$, T, and ρ; that is, it is a function of only v and the Hamiltonian of the system. All T and ρ dependencies are contained with $\{\psi_j\}$, as shown explicitly

in eq 12. What remains is to determine $\{\omega_j\}$ along with the T and ρ dependence of $E_{\sigma j}$ for a given choice of v. Determination of the former will be addressed in the following subsection. Treatment of the latter is motivated by the results in section 4 and is presented there.

Limiting Case for $\{\psi_j\}$ and a Method for Directly Enumerating $\{\omega_j\}$ from MC Simulations. The derivations above are general for a pure fluid and can be extended to mixtures in a straightforward, albeit algebraically tedious, manner.[36] They do not mandate the traditional approximations of treating a fluid as a coarse-grained or lattice system, except as required for practical implementation if one must enumerate $\{\omega_j\}$ for reasonably sized v, even if one does adopt the common simplification of $E_\sigma = 0$. However, if one had a general means to determine or accurately estimate $\{\omega_j\}$ or $\omega_v(n, E_n)$ for any system of interest, this would greatly facilitate the application of QC models to more complex systems than previously deemed tractable. Implementation within the $E_\sigma = 0$ approximation would then be straightforward with traditional QC treatments and would also provide a starting point for the development of improved QC models such as the one described here, in which the $E_\sigma = 0$ constraint is relaxed.

To illustrate the approach adopted here, we first consider the athermal or infinite temperature limit of the bcc-LG test system employed in section 4. This limit is chosen for the following two reasons: $\beta E_\sigma = 0$ by definition, and therefore the QC approximation becomes exact within numerical precision (see also section 4), and the limiting ψ_j distribution, $\{\psi_j^\infty\}$, is known exactly

$$\psi_j^\infty = \psi(n_j; \rho) = (1-\rho)^{(v/v_0 - n_j)}\rho^{n_j} \tag{20}$$

with ρ denoting the dimensionless lattice density defined in section 2. Given that both of these conditions are met, the key step is then to realize that we may generate a Markov chain of configurations within the limiting (athermal) ensemble, while simultaneously collecting statistics on the observed $p(n, E_n; v)$ for the Hamiltonian of interest. The $p(n, E_n)$ or p_j that will be observed is then given by

$$p_j^{\text{obs}} = \omega_j^{\text{obs}}\psi_j^\infty \tag{21}$$

Thus, estimates of $\{\omega_j\}$ for the Hamiltonian of interest can be obtained from eq 21 with the known $\{\psi_j^\infty\}$ and the measured $\{p_j^{\text{obs}}\}$. Improved estimates are obtained simply by running longer simulations to gather more accurate estimates of $\{p_j^{\text{obs}}\}$. That is,

$$\frac{p_j^{\text{obs}}}{\psi_j^\infty} \rightarrow \omega_j(\text{true}), j = 1, \ldots, m_c \tag{22}$$

should hold as the length of the Markov chain in the athermal ensemble increases.

For the bcc-LG system, the number of distinguishable configurations, $j = 1, \ldots, m_c$, is relatively small ($\sim 10^2 - 10^4$) even for reasonably sized v, and thus, highly precise estimates of ω_j can be obtained for all j. For molecular systems with continuous interaction potentials, one anticipates it will be necessary to discretize or bin energies within reasonably small intervals dE and the number of distinguishable cell states, m_c, will be prohibitively large for exact enumeration of all members of $\{\omega_j\}$. Rather, it is expected that eq 22 and an approach such as that above can provide valuable constraints on estimates of the true $\{\omega_j\}$, which would then be obtained by application, for example, of statistical methods to optimize the predicted (continuous) distribution $\omega_v(n, E_n)$ for a given Hamiltonian.

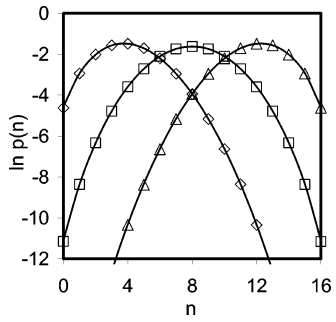

Figure 1. Subvolume occupancy distributions as a function of ρ for cells with $v/v_0 = 16$ in the athermal lattice gas. The symbols denote results from histograms gathered from *NVT* simulations: $\rho = 0.25$ (diamonds), 0.5 (squares), and 0.75 (triangles). The curves are predictions from the QC model with $E_\sigma = 0$ and the cell configuration degeneracies $\{\omega_j\}$ determined from eq 20 and the $p(n)$ data from only the $\rho = 0.5$ simulation.

TABLE 1: List of Estimated and Exact Cell Degeneracies for Athermal Lattice Gas and of Summation across Estimated Cell Degeneracies at Fixed *n* for the bcc-LG[a]

n_j	estimated ω_j	exact ω_j	$\Sigma_{E_n} w(n, E_n)$ in the bcc-LG
0	1	1	1
1	15	16	15
2	115	120	116
3	551	560	548
4	1811	1820	1798
5	4379	4368	4345
6	8082	8008	8008
7	11613	11440	11474
8	13095	12870	12921
9	11659	11440	11474
10	8142	8008	8008
11	4429	4368	4347
12	1838	1820	1797
13	563	560	548
14	119	120	118
15	16	16	16
16	1	1	1

[a] The volume of the cell is 16 sites.

4. Results and Discussion

Figure 1 displays density fluctuations measured directly in the $v/v_0 = 16$ cell for the athermal bcc-LG ($\epsilon = 0$ in eq 1) as a function of bulk density, in the form of $p(n)$ distributions. The symbols were determined from histograms collected during the *NVT* simulations. The curves are the results of solving eqs 18 and 19 simultaneously for each ρ value, using the set of ω_j determined using eq 22 and $p(n)$ gathered from a single simulation at only $\rho = 0.5$. The resulting set of estimated ω_j values is given in Table 1, along with the corresponding n_j values. The exact values of each ω_j for the athermal system are simply the corresponding binomial coefficients, and are shown in Table 1 for comparison to the estimated values determined from eq 22.

Despite the athermal system being rather simple, the results in Figure 1 and Table 1 suggest the procedure outlined in section 3 can reliably estimate $\{\omega_j\}$ provided sufficiently long simulations can be performed. It is notable that, despite the inaccuracies in the estimated degeneracies, the predicted $p(n)$ values are essentially indistinguishable from those observed directly in the simulations or those predicted using the exact degeneracies for

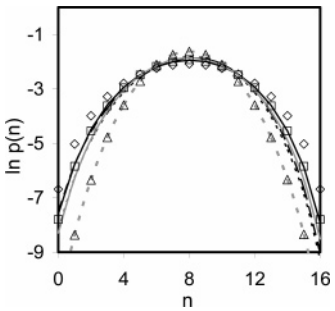

Figure 2. Subvolume occupancy distributions as a function of T for cells with $v/v_0 = 16$ in the bcc-LG at $\rho = 0.5$. The symbols denote results from histograms gathered from *NVT* simulations, and the curves denote predictions from the QC model. For $T^* = 1.92$, the simulation results are given by diamonds, the QC results with $E_\sigma = 0$ are given by the black dashed curve, and the QC results with the E_σ correction are given by the solid black curve. For $T^* = 2.4$, the simulation results are given by squares, the QC results with $E_\sigma = 0$ are given by the black dotted curve, and the QC results with the E_σ correction are given by the solid gray curve. For $T^* = 16.67$, the simulation results are given by triangles and the QC results with $E_\sigma = 0$ by the gray dashed curve. The QC predictions including the E_σ correction are indistinguishable at $T^* = 16.67$ from those with $E_\sigma = 0$.

the athermal bcc-LG, suggesting highly accurate estimates of ω_j values are not critical to achieve accurate predictions of density fluctuations as a function of ρ.

The procedure just described, and implied by eq 22, was next applied to the bcc-LG with *nn* attractions included ($\epsilon > 0$). p_j^{obs} values were obtained from athermal simulations at bulk densities of 0.25, 0.5, and 0.75, during which statistics on $[n_j, E_{n,j}]$ for cells with $v/v_0 = 16$ were collected throughout the course of ensemble averaging. In this way, a total of 148 distinguishable pairings of n_j and $E_{n,j}$ were identified ($j = 1, 2, \ldots, m_c$; $m_c = 148$), and their associated ω_j values were determined from eq 22 with $\psi_j = \psi_j^\infty$ (eq 20) for the given ρ of the overall system. In the interest of conserving space, the complete listing of $\{\omega_j\}$, $\{E_j\}$, and $\{n_j\}$ is not shown here but is available in the Supporting Information. As a simple check on these estimates of $\{\omega_j\}$ for the bcc-LG, the sum of $\omega_v(n, E_n)$ across E_n for each n should equal the values obtained for subcell degeneracies in the athermal limit. This quantity is also given in Table 1, showing good agreement with the exact values, as expected on the basis of the results in Figure 1.

Using this set of $\omega(n_j, E_{n,j})$ for the bcc-LG, and neglecting E_σ contributions for the moment, eqs 18 and 19 were solved to give $p(n)$ as a function of T and ρ. Figure 2 shows the predicted and observed density fluctuations in the $\rho = 0.5$ bcc-LG as a function of temperature for a range of values above the vapor−liquid critical point, with the critical temperature, T_c^*, estimated to be ~1.8 (see also Figure 3). Recall, in the 2000-site *NVT* simulations, for T below about T_c, frustrated phase separation occurs if the bulk density, ρ, lies between the densities of the coexisting vapor and liquid phases. This precludes sampling p_j representative of a homogeneous fluid at $\rho = 0.5$ except at $T > T_c$.

In Figure 2, the symbols indicate the local density distributions determined directly from *NVT* simulations for $v/v_0 = 16$ cells. The curves are solutions to eqs 18 and 19, utilizing $\{\omega_j\}$ determined above for the bcc-LG. Curves for both $E_\sigma = 0$ and those including an approximate E_σ value are shown. Those corresponding to the QC predictions with $E_\sigma = 0$ show very little temperature dependence and in this way deviate significantly from the observed $p(n)$ as T^* is reduced toward T_c^*. It is argued that these deviations are a direct result of the neglect of boundary contributions to the cell energies, which would tend

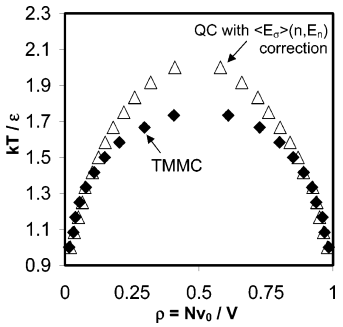

Figure 3. Temperature−density projections of the vapor−liquid phase boundaries for the bcc-LG determined from TMMC in the grand canonical ensemble (diamonds) and from the QC model with boundary interactions (triangles).

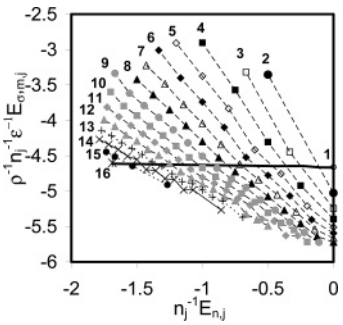

Figure 4. Correlations in E_n, n, and E_σ for the bcc-LG sampled under athermal conditions. $n_j^{-1}E_\sigma$ values are rescaled by ρ to provide density-independent profiles. The numbers 1−16 indicate the values of n_j for each profile. Additional details are given in the text.

to stabilize more rarefied, higher E_n cell arrangements as T is reduced and would also tend to encourage higher density, more highly coordinated local cell packings at the expense of lower density packings near the mode of the distribution. Both of these effects, neglected in the $E_\sigma = 0$ approximation, would be anticipated to increase the values of $p(n)$ on the wings of the distribution and are in qualitative agreement with the observed discrepancies seen in Figure 1.

Figure 4 illustrates the correlations in E_n and E_σ determined directly from the histograms of $[n, E_n, E_\sigma]$ gathered in the athermal *NVT* simulations described above. The average or mean boundary energy, $E_{\sigma,m,j}$, at fixed $(n_j, E_{n,j})$ from the athermal simulations is

$$E_{\sigma,m,j}(n_j, E_{n,j}) = \sum_{E_\sigma} E_\sigma p^{\text{obs}}(E_\sigma; n_j, E_{n,j}) / \sum_{E_\sigma} p^{\text{obs}}(E_\sigma; n_j, E_{n,j}) \tag{23}$$

and was calculated for histograms gathered at $\rho = 0.25$, 0.5, and 0.75. $E_{\sigma,m,j}$ is used rather than the true $E_{\sigma,j}$ (eq 11) as the statistics were gathered in the athermal ensemble, and the E_σ values for a given $(n_j, E_{n,j})$ were found to be narrowly distributed about the average value, $E_{\sigma,m,j}$, for each j. Such an approximation is not expected to hold as a function of temperature or for Hamiltonians based on strong nonisotropic interactions. It was further found that, by rescaling the $E_{\sigma,m,j}$ values by the inverse of the bulk density at which they were gathered, the observed correlations between $E_{n,j}$ and $E_{\sigma,m,j}$ were virtually superimposable at any density. Figure 4 displays the mean values of $\rho^{-1}n_j^{-1}E_{\sigma,m,j}$ for each $n_j^{-1}E_{n,j}$ value in the bcc-LG set of subcell configurations. The standard deviation for each point in Figure 4 is smaller than the size of its symbol, which follows from the narrowly

distributed E_σ values noted above. The dashed lines are included solely as guides to the eye and connect points with a common value of n_j. The value of each n_j is indicated by the number beside each line. The solid curve in Figure 4 is a plot of $E_{\sigma,m,j}$ averaged over all $E_{n,j}$ for a given n versus the average E_n for that value of n (=0, 1, ... , 16). Both quantities are functions of n alone.

Taken together, these results lead to the following conclusions regarding the contributions of the boundary energy to the overall energy of a given cell configuration. First, we see there is a relatively simple correlation between $E_{\sigma,m,j}$ and $E_{n,j}$ for a fixed n, and this is common across densities once one scales the magnitude of $E_{\sigma,m,j}$ by the bulk density. This latter observation is intuitively appealing, as one would anticipate the probability of having (orientation-independent) boundary interactions would be directly proportional to the number density of the surrounding medium for a given cell configuration. Further, the negative slopes of the constant-n profiles in Figure 4 indicate a negative correlation between the internal cell energy, $E_{n,j}$, and the corresponding boundary energy, $E_{\sigma,m,j}$. Physically, this compensating effect of $E_{\sigma,m,j}$ and $E_{n,j}$ on E_j can be understood by realizing that, at a fixed n_j value, increasing $E_{n,j}$ for a fluid with isotropic short-ranged interactions corresponds to configurations with an increasing number of particles sequestered toward the boundary. That is, the particles within the cell must give up contacts with other particles within the cell, and this leads to an increased probability of participating in contacts with particles on the subvolume surface. This interpretation is also consistent with the diminishing slope of $E_{\sigma,m,j}$ versus $E_{n,j}$ with increasing n_j, as increasing cell density decreases the number of feasible packing arrangements that differ significantly in the number of molecular contacts that are made within the cell versus those made across the cell boundary. Note that both of these results occur within a simulation producing an athermal Markov chain of configurations. Therefore, they arise simply from packing or entropic effects due to constraining particles within the cell to sit at the boundary and thus should be functions of only density for this system.

The results just presented motivate the following incorporation of $E_{\sigma,m,j}$ into the $p(n_j, E_j)$ calculations. Specifically, we define $\langle\epsilon_\sigma\rangle_j = \rho^{-1}n_j^{-1}E_{\sigma,m,j}$. This quantity is a function of only j. Its values versus j are given parametrically via n_j, $E_{n,j}$ in Figure 4. Substituting $E_{\sigma,m,j}$ for E_σ in eq 13 gives

$$E_j(\rho) = E_{n,j} + n_j\rho\langle\epsilon_\sigma\rangle_j \tag{24}$$

Equation 24 implicitly incorporates the density and j dependence of the boundary energy into the ψ_j calculations via eqs 18 and 19, and subsequently into the calculations of $p(n)$ and the QC EoS. The $p(n)$ predictions that result from the inclusion of eq 24 in the solution of eqs 18 and 19 are shown in Figure 2 for $\rho = 0.5$. Accounting for the boundary energy contributions in this manner makes significant improvements to the predicted $p(n)$ profiles. The agreement between predicted and directly observed profiles diminishes with decreasing temperature, suggesting temperature effects on the $E_n - E_\sigma$ correlations are significant and should be included for quantitatively accurate predictions of cell density fluctuations at lower temperatures.

The $E_n - E_\sigma$ correlations presented above, and included in eq 24, necessarily neglected temperature effects, as the statistics were gathered during athermal simulations. Although a detailed study of the temperature effects is beyond the scope of the present report, some preliminary findings are worth discussing. Figure 5 shows an $E_n - E_\sigma$ diagram, constructed as in Figure 4, from the $[n, E_n, E_\sigma]$ histogram gathered for the bcc-LG fluid

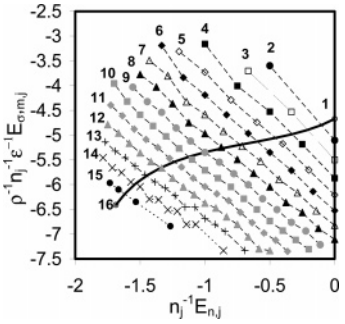

Figure 5. Correlations in E_n, n, and E_σ for the bcc-LG sampled at $T^* = 1.92$ and $\rho = 0.5$. All nomenclature and symbols are the same as those in Figure 4.

at $T^* = 1.92$ and $\rho = 0.5$. Many of the qualitative features of Figure 4 are retained in Figure 5, including the relatively simple linear form of the constant n profiles and the negative correlation between $E_{n,j}$ and $E_{\sigma,m,j}$. However, unlike the athermal results, the effects of temperature are manifest in the shifts of the higher cell density (higher n) profiles to lower average $E_{\sigma,m,j}$ values and the increase in the magnitudes of the slopes of the higher cell density profiles of $E_{\sigma,m,j}$ versus $E_{n,j}$ compared to the athermal case. Notably, the profiles for the more rarefied cells (i.e., as $n \rightarrow 0$) are essentially unchanged compared to the athermal results in Figure 4. Physically, this is consistent with a picture in which, upon decreasing temperature, the presence of particles at the inner cell boundary stabilizes an increased density of particles at the external surface of the cell due to the favorable attractive energies involved and in which the entropic penalties associated with sequestering molecules to the cell boundary diminish as T is lowered. Finally, it is interesting to note that the degree of improvement in the predicted $p(n)$ is asymmetric with respect to n but in a counterintuitive way. On the basis of the argument given above, one would anticipate that neglect of the temperature dependence of the $E_n - E_\sigma$ correlations would significantly underpredict the propensity for higher density cell configurations to form spontaneously in the fluid as temperature decreases. The $E_n - E_\sigma$ profiles in Figure 5 are relatively insensitive to temperature for low n, so one might expect the low cell density limit to be relatively insensitive to temperature. The results in Figure 2 clearly show this is not the case. This can be rationalized by realizing that an increase in the propensity for high density cell configurations requires a concomitant increase in the probability of rarefied cell configurations if the temperature changes occur at a constant (bulk) density and, further, that the changes in Figure 2 are on a logarithmic scale. Thus, relatively small increases in the high-n wing of the $p(n)$ distributions would likely require significantly greater relative increases in the low-n portion of the $p(n)$ profiles on the scale of the figure. One may speculate that incorporation in the future of the temperature dependence of the energy correlations will improve the predictions regarding cell density fluctuations at both high and low cell densities as temperature is decreased.

As a further test of the model predictions and the importance of incorporating boundary energy contributions into the QC model, the VLE phase boundaries of the bcc-LG were calculated using the QC EoS, with and without contributions of the boundary energy, that is, eq 22 with and without the $\langle\epsilon_\sigma\rangle_j$ term. Vapor and liquid saturation densities were identified at a given T^* by imposing an equal-area construction on the chemical potential as a function of density, which is equivalent to ensuring the pressure is the same in the vapor and liquid phases. These calculations require knowledge of $\mu(T, \rho)$, which follows

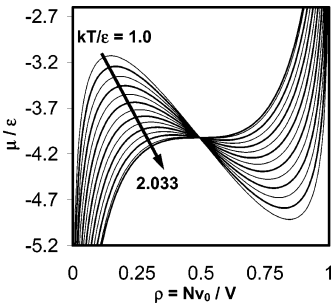

Figure 6. Isotherms of chemical potential vs density for the bcc-LG, calculated from the QC model with boundary interactions. The coexisting densities of liquid and vapor from the QC model in Figure 3 were determined from identifying the value of μ/ϵ that satisfies an equal-area construction to ensure the pressures in the two phases are equal.

from eq 15 and the formal relationship $\mu = (\partial a/\rho)_T$.[11] For the bcc-LG, this is given by

$$\frac{\mu}{kT} = \ln\frac{\rho}{1-\rho} + v^{-1}\left\{-\sum_j \omega_j \left(\frac{d\psi_j^{\infty}}{d\rho}\right)(1+\ln\psi_j^{\infty}) + \frac{\beta(E_0 - E_1) - \ln r_1}{(\rho_0 - \rho_1)}\right\} \quad (25)$$

Figure 6 displays isotherms of chemical potential versus density calculated using the average cell boundary energy approximation described above. The agreement between the TMMC results and those of the improved QC EoS are in excellent agreement at T/T_c values $< \sim 0.82$. The VLE predictions become increasingly less accurate at higher T, presumably because the vapor−liquid critical point is being approached, and the dimensions of the 16-site cell are much smaller than the length scale of the fluctuations as T_c is approached.

Finally, we note that in the absence of the boundary energy correction ($E_\sigma = 0$) VLE is never predicted to occur at finite temperatures in the QC EoS,[45] as evidenced by monotonic $\mu(\rho)$ at all T^* (results not shown). This last result highlights and reinforces the importance of including boundary energy contributions in subvolume or cell-based predictions as well as in the determination of macroscopic phenomena such as VLE from QC or similar cell-based equations of state.

5. Conclusions

A quasi-chemical, single-component fluid model is presented, including a simple semiempirical incorporation of subcell boundary interactions motivated by energy and density correlations from computer simulations of a simple liquid. At the athermal level at which they are included here, the boundary interactions exhibit dependencies on only bulk density and the subcell occupancy and internal energy fluctuations. These effects are easily incorporated into the traditional quasi-chemical fluid model framework and shown to accurately predict vapor−liquid equilibrium over a broad range of temperatures for a single-component fluid. The framework presented here for quasi-chemical models including cell boundary interactions provides not only the infinite dilution solvation properties of simple solutes in single-component solvents from $p(n)$[3,4] but also the equation of state for the solvent. The approach developed here, in which athermal simulations are used to enumerate cell configurations, circumvents the need to exhaustively enumerate individual cell configurations by hand, which has severely limited the utility of cell-based models for realistic fluids. On the basis of the ability of the present model to capture nontrivial effects of temperature and density on subcell density fluctuations and vapor−liquid phase equilibrium, it appears promising to extend the treatment to more complex systems such as water and mixed hydrogen-bonding solvents.

Acknowledgment. Grateful acknowledgment is made to the Donors of the American Chemical Society Petroleum Research Fund, for partial support of this research.

Supporting Information Available: Compilation of the complete $\{\omega_j\}$, $\{E_{n,j}\}$, and $\{n_j\}$ sets determined for the bcc-LG in tabular form. This material is available free of charge via the Internet at http://pubs.acs.org.

References and Notes

(1) Karplus, M. *Biopolymers* **2003**, *68*, 350−358.
(2) Paulaitis, M. E.; Pratt, L. R. *Adv. Protein Chem.* **2002**, *62*, 283−310.
(3) Reiss, H.; Frisch, H. L.; Lebowitz, J. L. *J. Chem. Phys.* **1959**, *31*, 369−380.
(4) Helfand, E.; Reiss, H.; Frisch, H. L.; Lebowitz, J. L. *J. Chem. Phys.* **1960**, *33*, 1379−1385.
(5) Stillinger, F. H. *J. Solution Chem.* **1973**, *2*, 141−158.
(6) Pratt, L. R.; Chandler, D. *J. Chem. Phys.* **1977**, *67*, 3683−3704.
(7) Debenedetti, P. G.; Raghavan, V. S.; Borick, S. S. *J. Phys. Chem.* **1991**, *95*, 4540−4551.
(8) Lazaridis, T.; Paulaitis, M. E. *Mater. Res. Soc. Symp. Proc.* **1992**, *278*, 319−324.
(9) Besseling, N. A. M.; Lyklema, J. *Pure Appl. Chem.* **1995**, *67*, 881−888.
(10) Besseling, N. A. M.; Lyklema, J. *J. Phys. Chem.* **1994**, *98*, 11610−11622.
(11) Roberts, C. J.; Debenedetti, P. G. *J. Chem. Phys.* **1996**, *105*, 658−672.
(12) Ashbaugh, H. S.; Paulaitis, M. E. *J. Phys. Chem.* **1996**, *100* (5), 1900−1913.
(13) Hummer, G.; Garde, S.; Garcia, A. E.; Pohorille, A.; Pratt, L. R. *Proc. Natl. Acad. Sci. U.S.A.* **1996**, *93*, 8951−8955.
(14) Truskett, T. M.; Torquato, S.; Debenedetti, P. G. *Phys. Rev. E* **1998**, *58*, 7369−7380.
(15) Soto-Campos, G.; Corti, D. S.; Reiss, H. *J. Chem. Phys.* **1998**, *108*, 2563−2570.
(16) Corti, D. S. *Mol. Phys.* **1998**, *93*, 417−420.
(17) Corti, D. S.; Soto-Campos, G. *J. Chem. Phys.* **1998**, *108*, 7959−7966.
(18) Truskett, T. M.; Debenedetti, P. G.; Sastry, S.; Torquato, S. *J. Chem. Phys.* **1999**, *111*, 2647−2656.
(19) Pratt, R.; LaViolette, R. A.; Gomez, M. A.; Gentile, M. E.. *J. Phys. Chem. B* **2001**, *105*, 11662−11668.
(20) Nezbeda, I.; Weinger, U. *Mol. Phys.* **2001**, *99*, 1595−1606.
(21) Eads, D. D. *J. Phys. Chem. B* **2002**, *106*, 12282−12290.
(22) Ashbaugh, H. S.; Truskett, T. M.; Debenedetti, P G. *J. Chem. Phys.* **2002**, *116*, 2907−2921.
(23) Truskett, T. M.; Dill, K. A. *J. Phys. Chem. B* **2002**, *106*, 11829−11842.
(24) D'Alessandro, M.; D'Abramo, M.; Brancato, G.; Di Nola, A.; Amadei, A. *J. Phys. Chem. B* **2002**, *106*, 11843.
(25) Apol, M. E. F.; Amadei, A. *J. Phys. Chem. B* **2003**, *107*, 1410.
(26) Pratt, L. R.; Ashbaugh, H. S. *Phys. Rev. E* **2003**, *68*, 021505.
(27) Putnam, R.; Taylor, R.; Klamt, A.; Eckert, F.; Schiller, M. *Ind. Eng. Chem. Res.* **2003**, *42*, 3635−3641.
(28) Sandler, S. I. *Fluid Phase Equilib.* **2003**, *210*, 147−160.
(29) D'Abramo, M.; D'Alessandro, M.; Amadei, A. *J. Chem. Phys.* **2004**, *120*, 5226.
(30) Hill, T. L. *Statistical Mechanics: Principles and Selected Applications*; Dover Publications: New York, 1956.
(31) Ben-Naim, A. *Statistical Thermodynamics for Chemists and Biochemists*; Plenum Press: New York, 1992.
(32) Errington, J. R. *J. Chem. Phys.* **2003**, *118*, 9915−9925.
(33) Singh, J. K.; Kofke, D. A.; Errington, J. R. *J. Chem. Phys.* **2003**, *119*, 3405−3412.
(34) Virnau, P.; Mueller, M. *J. Chem. Phys.* **2004**, *120*, 10925.
(35) Ytreberg, F. M.; Zuckerman, D. M. *J. Chem. Phys.* **2004**, *120*, 10876.
(36) Roberts, C. J. Unpublished work.
(37) Roberts, C. J.; Panagiotopoulos, A. Z.; Debenedettti, P. G. *Phys. Rev. Lett.* **1996**, *77*, 4386-4389.

(38) Allen, M. P.; Tildesley, D. J. *Computer Simulation of Liquids*; Oxford University Press: Oxford, U.K., 1989.

(39) It can be shown that it is necessary to have the number of layers in the vertical or *z*-direction be double those in the horizontal plane and to have an even number of sites along each side to ensure each of the four simple cubic sublattices present in a bcc lattice are equally represented.[37]

(40) Wilding, N. B. *Phys. Rev. E* **1995**, *52*, 602−611.

(41) Rovere, M.; Heermann, D. W.; Binder, K. *J. Phys.: Condens. Matter* **1990**, *2*, 7009.

(42) Kaski, K.; Binder, K.; Gunton, J. D. *Phys. Rev. B* **1984**, *29*, 3996.

(43) Layn, K. M.; Debenedetti, P. G.; Prud'homme, R. K. *J. Chem. Phys.* **1998**, *109*, 5651−5658.

(44) If one foregoes the need to determine the EoS and instead seeks only $\{p_j\}$, the problem is reduced to determining m_c-2 unknowns and it is possible to apply the constraints of eqs 13 and 14 along with another suitable constraint such as maximizing the information entropy associated with the estimate of $\{p_j\}$.[13]

(45) There is a subtle point to be clarified with traditional QC EoS calculations. Namely, N_c/V is not always taken as equivalent to the υ value of the subcell that has its internal configurations enumerated. That is, an effective υ value is used for rescaling the summations across j in the EoS expressions so as to account for the lack of boundary interactions. In such cases, N_c/V is typically smaller than the true subcell volume and is chosen to make the total number of *nn* contacts per site match the exact result for the lattice of interest. If one utilizes this ad hoc and inherently inconsistent procedure to compensate for the lack of boundary interactions in the bcc-LG, it is possible to force the EoS to display VLE, but the boundaries are significantly skewed from the true values.